Strong Planar Shock Waves Generated by Explosively-Driven Spherical Implosions

I. I. GLASS,* AND S. K. CHAN†
University of Toronto, Toronto, Canada
AND
H. L. BRODE‡
R & D Associates, Santa Monica, Calif.

Implosions were used to raise the pressure and temperature of a driver gas to extreme values. Strong planar shock waves were thereby generated. A theoretical and experimental study was conducted on the performance of a 2.54-cm-diam shock tube driven by a 20-cm-diam hemispherical implosion driver. The analytical performance of the shock tube was predicted by numerically solving the set of governing nonlinear partial differential equations including appropriate loss mechanisms in the different regimes of the flow. The actual performance of the shock tube was determined experimentally by monitoring the shock velocity, flow uniformity, and test time for different driver conditions. These included stoichiometric hydrogen-oxygen mixtures with and without a PETN explosive liner. Planar shock waves were produced up to 11 km/sec without PETN and up to 19 km/sec with the addition of only 113 g of PETN explosive. Uniform test times of about 2-1 μsec were available at a distance of 3.3 m from the diaphragm (where the shock velocities were now 9 and 14 km/sec).

1. Introduction

WITH the advent of unmanned and manned planetary space explorations great demands were made for advanced hypervelocity test facilities in order to simulate planetary entry and meteoroid impact conditions. It became apparent that the existing hypervelocity facilities, such as shock tubes and launchers were incapable of simulating the anticipated planetary entry velocities (e.g., Jovian entry velocity of up to 60 km/sec, Ref. 1).

In the past few years considerable efforts were expended towards extending the capabilities of existing facilities and to develop new devices based on novel ideas. Recently Menard[2] reported some improvement on an electrically-driven shock tube which enabled the device to drive shock waves of 45 km/sec with little attenuation. Previously the conventional shock tubes seemed to have reached a performance limit of about 15 km/sec (Ref. 3). In order to overcome this velocity plateau, a number of new devices[4-8] were conceived and built based on the use of high-explosives, which are capable of providing high-energy density at moderate cost. For example, one gram of PETN (1 g/cc) contains approximately 5.5 kjoules of energy. A large electrical capacitor capable of storing an equivalent amount of energy would cost about $2000 compared with a fraction of a cent for the explosive. Although this is an oversimplification in the application of both types of energy storage it nevertheless illustrates the point.

The capability of explosive-driven shock tubes has long been recognized. Savitt and Stresau[9] and Schreffler and Christian[10] are among the earliest reported of an explosive-driven shock tube. Both devices generated the shock directly from a piece of detonating cylindrical solid explosive (Fig. 1a). More sophisticated

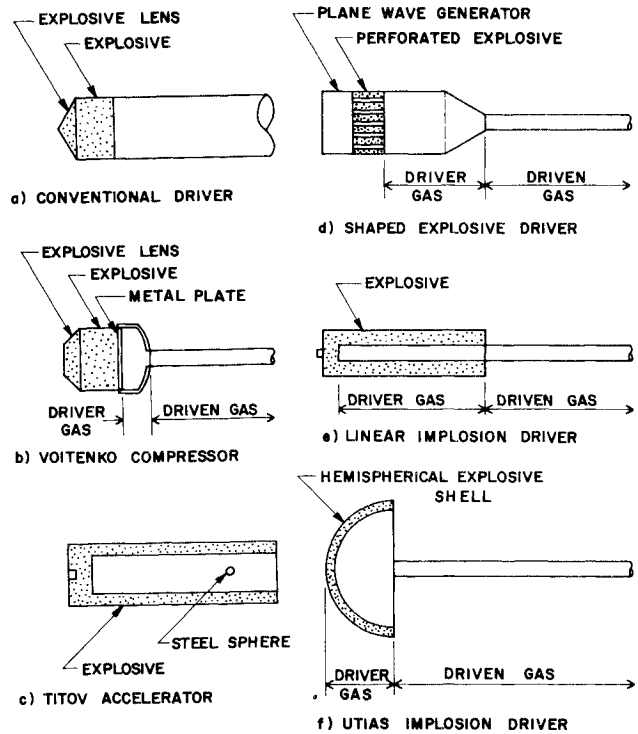

Fig 1 Schematic diagram of the configurations of different explosive-driven facilities.

Received June 18, 1973; revision received October 22, 1973. We wish to thank G. N. Patterson for his encouragement during the course of this work. We appreciate P. Crouse for his invaluable help in conducting the experiments and A. Perrin for his assistance in the design and construction of the electronic equipment. We are indebted to W. Czerwinski for his assistance and suggestions in the design of the implosion driver. The discussions with W. O. Graf were useful and stimulating. The work was financially supported by AFOSR (USA Grant AFOSR 72-2274) and by NRC (Canada).

Index categories: Reactive Flows; Shock Waves and Detonations; Boundary Layers and Convective Heat Transfer—Turbulent.

* Professor and Assistant Director, Institute for Aerospace Studies. Associate Fellow AIAA.

† Institute for Aerospace Studies; presently Research Physicist at Explosives Research Laboratory, Canadian Industries Ltd., McMasterville, Quebec, Canada.

‡ Program Manager.

set-ups were built in the last several years. Figures 1b–f show symbolically the operating principles of some of these explosive-driven devices. In the Voitenko compressor (Fig. 1b) (Refs. 4 and 5), a block of explosive drives a metal plate into a converging cavity compressing the driver gas, which is used to drive strong shock into the shock-tube channel. The device used by Titov et al.[6] (Fig. 1c) is mainly used to accelerate, by means of aerodynamics drag, solid projectiles to hypervelocities. It consists of a tube of explosive with the projectile suspended in the centre of the tube. In the shaped-explosive driver developed by Cowan[7] (Fig. 1d), channeled solid explosive is used to enhance the initial velocity of the driver gas which then undergoes further compression passing through a converging geometry before reaching the shock tube. In the linear-implosion driver developed by Gill et al.[8] (Fig. 1e), the driver tube is progressively collapsed by the detonating explosive which surrounds it and drives a planar shock ahead of the collapsing. tube. The driver gas velocity can be double that of the explosive detonation velocity if jetting occurs. The UTIAS explosive-driven implosion driver developed by Glass et al.[11] is shown in Fig. 1f.

The operation of the UTIAS device utilizes a hemispherical implosion to increase the pressure and temperature of the predetonated driver gas that is required to generate shocks at hypervelocities. The sequence of operation is shown in Fig. 2. A detonation is generated in a stoichiometric hydrogen-oxygen mixture at the geometric center of the hemisphere by using a fine, short exploding copper wire (4 mil diam × 2.5-mm long) as an initiator. The hemispherical detonation wave moves towards the periphery (Fig. 2a) and reflects from a shell of PETN explosive placed against the wall of the cavity. The explosive shell is simultaneously and impulsively initiated thereby driving a stable, focussed implosion into the preheated and compressed hydrogen-oxygen detonation products (Fig. 2b) and reflects from the origin leaving a pocket of gas at extreme pressures and temperatures that can be used to drive a shock wave in a channel or a projectile in a launcher barrel. In comparison with the other explosive facilities, the UTIAS driver is a safe, compact, self-contained and reusable facility.

Preliminary investigations on an 8-mm-diam shock tube were carried out and results were reported by Glass and Poinssot.[12] The present theoretical and experimental analysis greatly extends

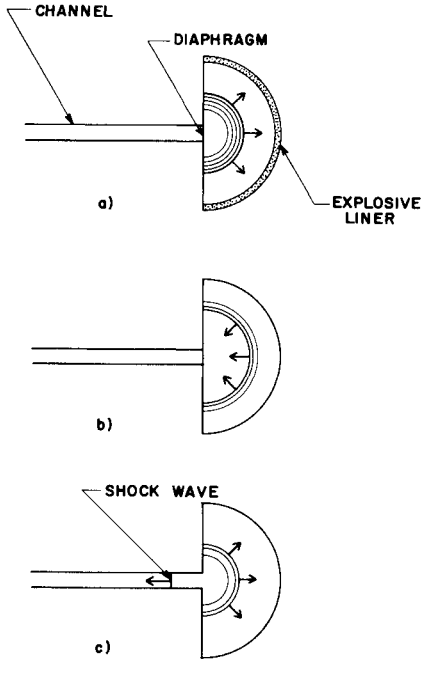

Fig. 2 Schematic diagram illustrating the principle of operation of the UTIAS implosion-driven shock tube: a) ignition and detonation; b) implosion phase; c) reflection and generation of shock wave in the channel.

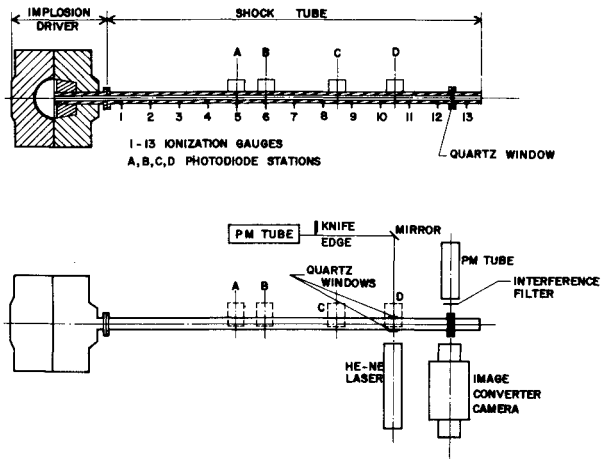

Fig. 3 UTIAS implosion-driven hypervelocity shock tube and instrumentation.

the work to a realistic 2.54-cm-diam shock tube driven by a 20-cm-diam hemispherical implosion driver. In addition to the exact numerical results a simplified solution also was developed allowing the maximum expected shock velocity to be predicted for a given set of initial conditions. The analysis indicates that it would be difficult to significantly increase shock velocities and flow durations by simply scaling up the equipment.

2. Experimental Equipment and Instrumentation

Basically the UTIAS Implosion-Driven shock tube consists of a 20-cm-diam hemispherical implosion driver and a 365-cm long, 2.54-cm-diam shock-tube channel separated by a scribed stainless steel diaphragm (Fig. 3). The shock-tube channel was made of thick-wall (5.4 cm o.d. × 2.54 cm i.d.) high-pressure steel tubing honed to 30 μ finish. The construction and operation of the implosion driver were fully described in Refs. 13 and 14. Briefly, the implosion driver consists of two parts, namely the front plate and the explosion chamber. A 20-cm-diam hemispherical cavity was machined in the explosion chamber block supporting the explosive linear package. In the explosive runs, a 20° conical liner plate was added to the planar face of the hemispherical cavity to give extra protection for the front plate section against any possible damaging off-centered implosion.[13,14]

The success of generating stable, focussed implosions depends strongly on the properties of the explosive liner. The present scheme of initiating the explosive (superfine PETN) by the gaseous detonation wave (stoichiometric mixture of hydrogen-oxygen at an initial pressure of 400 psi) has proven to be most promising[15] and was used in all explosive runs in the present study. One major drawback of superfine PETN is its lack of mechanical binding strength by itself and manufacture of a homogeneous explosive shell with close dimensional tolerances was proved to be difficult.[13] For the present series of experiments, the superfine PETN powder was mixed with 1.5% of cotton linters with water forming a slurry which was then pushed into a preformed shell of open-core plastic foam glued onto a copper liner inner surface. The package was then air dried very slowly. This way the explosive package had sufficient strength to withstand handling and the impact of the gas jet during loading of the driver with sufficient homogeneity to ensure stable, focussed implosion. (More details on the explosive package can be found in Refs. 13 and 16).

Unlike a conventional shock tube where the exact time the diaphragm starts to open is not critical to the operation, the implosion driver is a dynamic system for which the timing of the implosion and the diaphragm opening is very critical. Although the postdetonation pressure was high (1000–5000 psi), it was not

practical to use thick nonmetallic diaphragms and let the implosion shatter it owing to the loss of driving energy. A compromise was found to use thin scribed stainless-steel diaphragm of known opening characteristics whereby it would begin to open before the arrival of the implosion wave which could then pass through with minimum obstruction. It could be shown[16] that the opening time, including diaphragm stretch, could be predicted and proper diaphragms chosen to have opening time comparable to the implosion time allowing the maximum shock velocities to be obtained from a given driver condition.

The instrumentation used is described in the following. Ionization gages installed at 30.5 cm intervals along the tube were used to detect the arrival of the shock front. Four photodiode (HP 5082-4220 PIN Photodiodes) detectors and associated electronics were installed on the tube as shown in Fig. 3. These photodiode detectors were used to monitor the arrival of the shock front and the light intensity of the luminous shock-heated driven gas. A laser-schlieren system was used to detect the shock front and the turbulent contact region providing a very positive way of defining the test time. The system was placed at 3.3 m from the diaphragm. It consisted of a 5 mw He-Ne laser, a knife edge and a photomultiplier detector whose output signal was monitored by an oscilloscope. Two 6.3-mm-diam windows were mounted on the tube to allow the laser beam to pass through the center of the tube. At 3.9 m from the diaphragm a washer shaped window was installed between the joints of the 365 cm section and a short section that connects to the dump tank. Two 0.5 mm wide slits were placed on opposite sides of the window. On one side the slit was 13 mm long viewed by a photomultiplier through a 5300Å ($\pm$25Å) interference filter. On the other side the slit span allowed observation of the entire cross section of the tube and was viewed by a TRW Image Converter Camera operated in a streak mode. The slit image was swept in the direction of the tube axis with time.

3. Theoretical Performance Predictions

3.1 Numerical Solutions

By using appropriate mathematical models it is possible to analyze the performance of the various phases of the implosion-driven shock tube. The flow in the implosion driver is spherically symmetric while that in the shock-tube channel is planar. Therefore with the exception of the short transition region from the hemispherical to the tube geometry, the entire driver-driven gas flow can be adequately described by the set of one-dimensional equations of motion. The simulation was made more realistic through the addition of appropriate loss mechanisms in the different regimes of the flow. An approximating one-dimensional geometry was used to represent the complex two-dimensional flow in the transition region from the hemispherical chamber to the shock-tube channel. This model allows the use of the same set of one-dimensional equations of motion to simulate the flow in the transition region without generating spurious shock and expansion waves.

3.1.1 *Equations of motion*

The one-dimensional equations of motion can be written in the following form:[17]

Continuity equation:

$$\partial m/\partial t = \dot{m} \tag{1}$$

Momentum equation:

$$(\partial u/\partial t) + A(\partial p/\partial m) = F \tag{2}$$

Energy equation:

$$(\partial e/\partial t) + p(\partial v/\partial t) = D \tag{3}$$

together with the equation of state

$$p = p(e, v) \tag{4}$$

where, m is the Lagrangian mass coordinate; $\dot{m}$ is the rate of change of mass of a zone used in the computation scheme; F represents the friction and body force term; D includes non-adiabatic effects from heat sources and sinks; A is the cross-sectional area of the tube.

Equations (1-4) can be transformed into a set of equivalent finite-difference equations which can be numerically integrated (see Ref. 18 for more details). The equations of state for air, the burned stoichiometric mixture of hydrogen-oxygen driver gas and the burned PETN explosive were described by Brode.[17,18] Shock discontinuities were handled by the addition of an artificial-viscosity pressure[19] to the pressure term, p, in Eqs. (2) and (3). The forms for the terms $\dot{m}$, F and D depend on the particular loss mechanisms to be included in the various parts of the flow. Inside the hemispherical implosion chamber wall effects are confined to a stagnant layer of gas adjacent to the walls, their effects on the main body of the driver gas would be small and were neglected in the analysis. On the other hand, for flow inside the shock-tube channel wall effects can become significant because of the relatively small 2.54 cm channel diameter.

3.1.2 *Driver gas region*

In the driver gas, the boundary layer formed at the entrance section of the shock-tube channel can become a fully-developed pipe-flow within 20 tube diameters[20] if the flow is turbulent. The high-pressure driver gas passing through the diaphragm station becomes a highly eddying and turbulent flow.[21] Therefore, a fully-developed, turbulent, pipe-flow model would be a reasonable representation of the driver gas flow in the entire length of the tube. This model was also used by Crowley and Glenn[4] to simulate their entire flow (driver as well as driven gas regions). In this model the wall friction is assumed to affect the entire core of the flow dragging the gas in a direction opposite to that of the flow. Turbulent heat loss to the wall is also included. The momentum and energy loss terms F and D in Eqs. (2) and (3), respectively, then become[4]

$$F = -(1/\Delta m)(C_f \tfrac{1}{2}\rho u^2 S) \tag{5}$$

$$D = (1/\Delta m)(C_f \tfrac{1}{2}\rho u^2 S|u| + \dot{W}) \tag{6}$$

where Δm is the mass of gas in a computational zone in the barrel with surface area S. C_f is the friction coefficient and $\dot{W}$ is the convective turbulent heat transfer rate given by

$$\dot{W} = -C_H \rho |u| S(e + pv) \tag{7}$$

The coefficient C_H is that for turbulent heat transfer (Station number) taken for simplicity as half the friction coefficient, using the Reynolds analogy

$$C_H = \tfrac{1}{2}C_f \tag{8}$$

C_f was taken to have a value of 0.002, which has been shown[22,23] to be more representative of shock-tube flows than the value (0.004) used by Crowley and Glenn[4] obtained from incompressible channel flow data.

3.1.3 *Driven gas region—boundary-layer mass-loss model*

While the turbulent pipe-flow model can be considered adequate for the driver-gas region, it is far from correct for the driven-gas region. For the present test-gas conditions with initial channel pressure p_1 at about 1 torr, the boundary layer developed behind the shock front can be assumed to remain laminar[24] and the boundary-layer thickness can be shown[16] to be less than 7% of the tube radius within the expected test gas length of a few centimeters. On the other hand, the corresponding negative displacement thickness δ^*, was of the order of 50% of the tube radius. In this region, therefore, a more appropriate model would be one which takes into account the effect of large negative δ^* values. The negative δ^* behaves like an aerodynamic sink removing mass from the inviscid core. This process generates expansion waves in the flow which attenuate the shock front,[25,26] accelerate the contact surface, reduce the available test time[24] and at the same time produce nonuniform test gas flow properties.[25] By incorporating the boundary-layer effects in a

numerical computation scheme it is theoretically possible to simulate flows behind actual attenuating shock waves.

It has been shown[25,27] that by integrating the governing equations across the tube diameter the appropriate averaged quantities outside the boundary layer satisfy the one-dimensional energy and momentum equations without viscous terms, but that a displacement term appears in the continuity equation. That is, as far as the mean flow quantities are concerned the energy and momentum equations remain identical to the inviscid case, while there is a new mass-loss term in the continuity equation. This mass-loss term will depend on the boundary-layer solutions. Knowing this term, it is then possible to simulate the flow by incorporating it into Eq. (1).

From Ref. 24, δ^* can be shown to be related to the local free stream density ρ_e and velocity u_e by

$$-\delta^* = (d/4)\{[(\rho_e u_e)_o - \rho_e u_e]/\rho_e u_e\} \tag{9}$$

where d is the hydraulic diameter. The local rate of mass loss per unit volume ($\dot{m}_v$) to the boundary layer at any station is related to δ^* by

$$\dot{m}_v = (4/d)\rho_e u_e(d\delta^*/dx_s) \tag{10}$$

where x_s is the distance from the shock front. For a laminar boundary layer, the development of δ^* is given by[28]

$$-\delta^* = \bar{\delta}^* x^{1/2}\left(\frac{p_{st}}{p_1}\right)^{1/2}\left(\frac{\mu_1}{\mu_{st}}\right)^{1/2}\left(\frac{T_1}{T_{st}}\right)^{1/4} \tag{11}$$

in which the subscript (st) stands for standard atmospheric conditions (290°K, 1 atm), the subscript (1) stands for conditions ahead of the shock and $\bar{\delta}^*$ is a function of M_s, ρ_e/ρ_1, u_s/u_e, p_e/p_1 as given in Ref. 28. By differentiating Eq. (11) we obtain

$$d\delta^*/dx_s = d\delta^*/dx = \tfrac{1}{2}\delta^*/x \tag{12}$$

The concept of local similarity was assumed. Substituting Eqs. (11) and (12) into Eq. (10) and rearranging

$$\dot{m}_v = \frac{2}{d}\rho_e u_e \frac{(\bar{\delta}^*)^2}{\delta^*}\left(\frac{p_{st}}{p_1}\right)\left(\frac{\mu_1}{\mu_{st}}\right)\left(\frac{T_1}{T_{st}}\right)^{1/2} \tag{13}$$

A closed form solution was given in Ref. 28 for $\bar{\delta}^*$ used in Eq. (13). Mirels[28] noted that the correlation formula used here for $\bar{\delta}^*$ agreed reasonably well with solutions for ionized boundary layer[29] up to shock velocity $u_s = 12$ km/sec. This is within the range of expected performance of the pure gas driver. For the explosive case, u_s values from 13 to 20 km/sec are expected. In this range the use of Mirels correlation formula is extended just beyond its proven range of validity. In any case, this would be a good first approximation in absence of more accurate solutions for the highly-ionized boundary layer.

According to the present boundary-layer mass-loss model, the loss terms $\dot{m}$, F and D in Eqs. (1–3) become

$$\begin{cases} \dot{m} = \dot{m}_v A\Delta x \\ F = 0 \\ D = 0 \end{cases} \tag{14}$$

in which Δx is the width of a particular zone in the numerical computation scheme.

3.1.4 Transition from hemispherical to planar tube geometry

Various attempts to formulate a proper one-dimensional transition[13] were made without much success in obtaining smooth flows through the region. The spherical-segment scheme[30] although it gave continuous zone-area change still has discontinuous jumps in the derivatives of the specific volume, which introduces spurious shock and expansion waves,[17] making the accuracy of the results uncertain. In order to eliminate these uncertainties, a completely continuous transition scheme was adopted having a continuous change of area and in the derivatives of specific volume across the entire transition region. Flow properties were found to change smoothly without any spurious shock and expansion waves. Complete details are giver in Ref. 16.

3.2 Simplified Solution

While the numerical solution provides detailed analysis and insight into the entire flowfield, nevertheless it is extremely time consuming (it takes approximately 25 min on an IBM 370-165 computer to run a complete case) and the results obtained apply only to the given set of initial conditions. In this sense it is desirable to have completely analytical or numerical-analytical solutions, which would allow one to predict the performance of the implosion driver for any given initial conditions.

It was found that the implosion process away from the hemispherical wall approaches a self-similar pattern[15,16] and the pressure, density and particle velocity immediately behind the imploding shock can be described by the following[16]

a) Pure Gas

$$p/p_i = 11.24\,(R/R_o)^{-0.58} \tag{15}$$

$$\rho/\rho_i = 1.2(R/R_o)^{-0.41} \tag{16}$$

$$u = 9.74\times 10^4 (R/R_o)^{-0.47}\ \text{cm/sec} \tag{17}$$

p_i and ρ_i are intial gas pressure and density before detonation. Equations (15–17) are independent of p_i and ρ_i.

b) Explosive Driver (400 psi)

$$p = 1.7\times 10^9\,(W/W_1)^{1/2}(R/R_o)^{-0.57} \tag{18}$$

$$\rho = 6.05\times 10^{-2}\,(W/W_1)^{1/4}\,(R/R_o)^{-0.28} \tag{19}$$

$$u = 3.62\times 10^5\,(W/W_1)^{1/4}(R/R_o)^{-0.32} \tag{20}$$

where $W_1 = 200$ g for hemispherical configuration; $W_1 = 131.59$ g for 140° conical chamber (with a liner) configuration is the reference weight of explosive. W is the weight of explosive, R_o is the chamber radius.

Equations (15–20) can be extended to the diaphragm section which can be shown[16] to have an equivalent radius

$$\begin{aligned} R &= R_H = d/2(2)^{1/2} \text{ for a hemispherical chamber} \\ R &= R_c = d/2(2)^{1/2}\,1/(1-\sin\theta)^{1/2} \text{ for a conical chamber} \end{aligned} \tag{21}$$

with included angle $(180° - 2\theta)$, d is the tube diameter. Therefore the pressure, density and particle velocity (p_4, ρ_4, and u_4, respectively) at the diaphragm station, are known from Eqs. (15–20). Assuming that the diaphragm opens instantaneously and that the flow undergoes an unsteady expansion, it can be shown[16] that the shock velocity u_s is given by the following implicit equation for a given set of p_4, ρ_4, u_4

$$\Gamma u_s = u_4 + \frac{2}{\gamma-1}a_4\left[1 - \left(\frac{\Gamma\rho_1 u_s^2}{p_4}\right)^{(\gamma-1)/2\gamma}\right] \tag{22}$$

where $\Gamma = (\rho_2/\rho_1 - 1)/(\rho_2/\rho_1)$ and ρ_2/ρ_1 is the density ratio across the shock front in the driven gas, γ is the effective adiabatic exponent ($\gamma \sim 1.15$ and 1.14 for a pure gas driver and explosive driver cases, respectively) and $a_4 = (\gamma p_4/\rho_4)^{1/2}$ is the sound velocity. Equation (22) can be readily solved with Eqs. (15–20) for any given explosive weight, tube diameter, chamber diameter and configuration, initial channel pressure (as ρ_1) for both pure gas and explosive driver and also for any given initial driver-gas pressure for the case of pure-gas driver.

4. Results

The implosion driver was operated in both the pure-gas and the gas-plus-explosive modes. The addition of an explosive liner was found to increase the performance capability of the implosion driver without basically changing the structure of the flow. The following analytical diagrams illustrating the flow structure for the explosive-gas driver mode are also typical of the pure-gas mode.

Figure 4 is a wave diagram embodying all the present refinements for a 140° conical driver chamber with 80 g PETN, 400 psi $2H_2+O_2$ driving into 1 torr air. The primary shock S is generated by the implosion wave IS by bursting the diaphragm at $x = 0$. The primary shock S is followed closely by the driver-driven gas contact surface CS and a number of secondary shocks (S_0, S_1, S_2, etc.) generated by the reciprocating shock wave inside

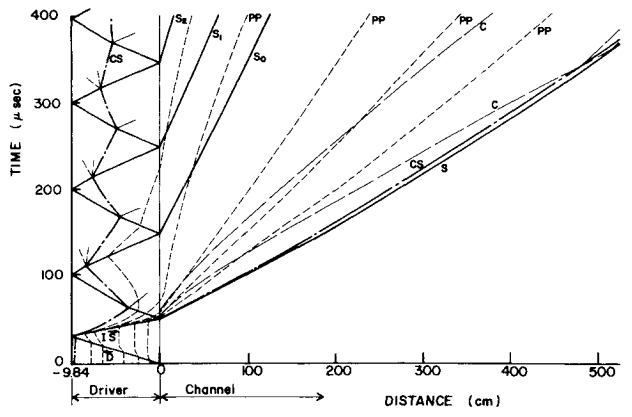

Fig. 4 Theoretical wave diagram of the implosion-driven shock tube. Conical (140°) driver chamber, 80 g PETN, 400 psi $2H_2 + O_2$, 1 torr air.

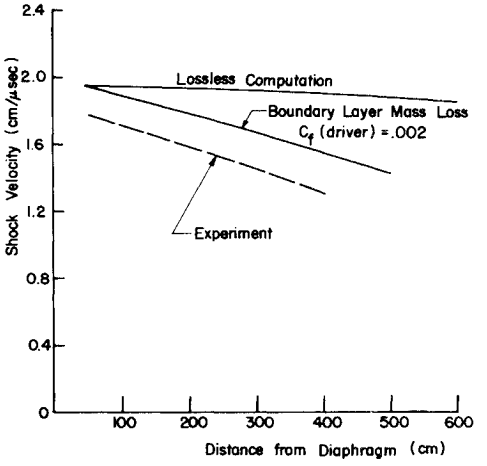

Fig. 6 Comparison of predicted and measured shock velocity variations with distance from diaphragm. Conical (140°) driver chamber, 80 g PETN, 400 psi $2H_2 + O_2$, 1 torr air.

the driver chamber. Also shown in the figure are a number of particle paths and characteristic lines. It can be seen that the distance between the primary shock S and contact surface CS approaches a small constant value[24,31] due to the effect of the boundary-layer leakage allowed for in the computation. The major differences between the wave diagram of this system and that of a simple shock tube are the existence of the secondary shocks.

Figure 5 shows the variation of particle velocities with distance at different times. At any given time the particle velocity is seen to increase from the shock front to the contact surface then decreases with distance except at the secondary shocks which cause a few bumps in the profile. The increase in particle velocity following the shock front S is due to the well-known effects of boundary-layer mass loss[24] which increases the interface velocity while attenuating the shock wave. The attenuation of the shock wave causes the peak particle velocity to decrease with distance and time. Similar curves can be plotted for the thermodynamic quantities (see Ref. 16 for details).

The attenuation of the shock velocity with distance is shown in Fig. 6, for a case of 400 psi initial driver pressure plus 80 g PETN driving into 1 torr air. Two computational solutions are presented showing the relative contributions to the rate of attenuation due to the driver and driven-gas loss-effects. The rate of attenuation agrees very well with analysis indicating the physical soundness of the tube-loss models used since the shock attenuation rate is independent of the diaphragm opening losses. The discrepancy between the magnitude of the predicted and the measured shock velocities was attributed to the shock formation and viscous losses[21] during the diaphragm opening process. The relative as well as absolute amount of this loss reduces with increase in driver pressure as will be shown later.

Figure 7 compares the predicted and experimental shock velocities of a pure-gas driver with different initial driver pressures and a fixed channel pressure of 1 torr. The circles are the experimental points while the triangles are numerical solutions for the corresponding initial driver pressure. The solid line is the simplified solution [Eqs. (22 and 15–17)]. There is excellent agreement between the simplified solution and the exact numerical solution. The difference between predicted and experimental values can be seen to decrease with increasing driver pressure as mentioned above. This phenomena of reduction of viscous formation losses with driver pressure has also been observed by Glass and Patterson.[21] Similar good results are

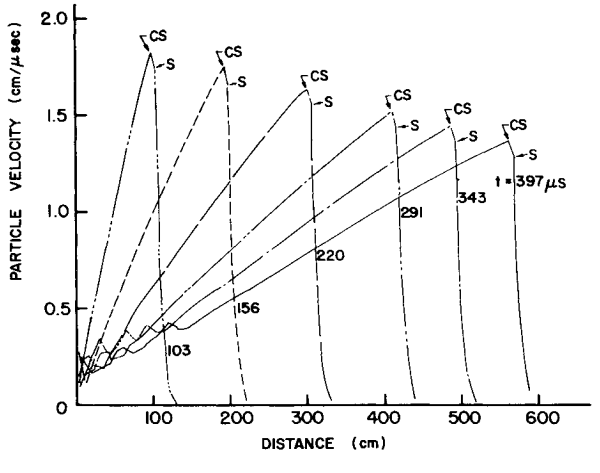

Fig. 5 Variation of particle velocity with distance at different times. Conical (140°) driver chamber, 80 g PETN, 400 psi $2H_2 + O_2$, 1 torr air.

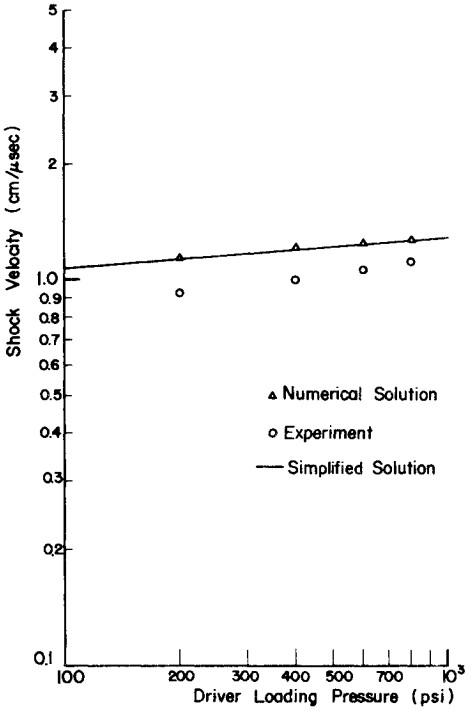

Fig. 7 Variation of shock velocity with initial driver pressure. (p_1 = 1 torr, shock velocity taken at 0.5 m from diaphragm.)

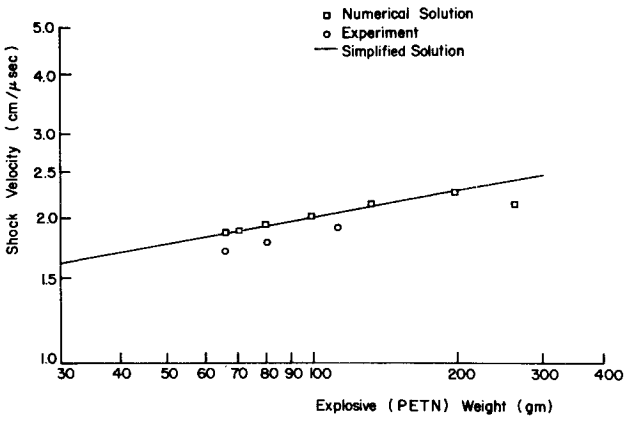

Fig. 8 Variation of shock velocity with explosive weight. [Conical (140°) driver chamber, 400 psi $2H_2+O_2$, 1 torr air.)

obtained for fixed driver conditions (no PETN) and varying initial channel pressures (see Ref. 16 for details).

Figure 8 shows the variation of shock velocity with explosive weight for a 140° conical implosion chamber configuration, 400 psi initial driver pressure, and 1 torr channel air. The experimental results fall within less than 8% below the predicted values from numerical and simplified solutions. Here the simplified solution was obtained by solving Eq. (22) together with Eqs. (18–20) and Eq. (21) for $\theta = 20°$. There is excellent agreement between the numerical and simplified solutions up to about 200 g of explosive (where the explosive liner has an optimum thickness to chamber radius ratio of about 0.1) beyond which nonsimilar effects[16] on the implosion wave properties are felt at the tube area and the efficiency of the driver drops.

Figure 9 shows the records of the signals from the laser-schlieren system (LS) and the photodiode detector (PD) at the same station from a) a 400 psi gas run, and b) an 80 g PETN and 400 psi run. The arrival of the shock front was detected showing a jump in signal from the laser schlieren system followed first by a period of quiescent flow then the turbulent contact region indicated by the rapidly oscillating signal. The LS detected the shock front as a positive spike in case (a) indicating a positive refractive index (or density) gradient through the non-equilibrium (NEQ) region. The corresponding region was far too short to be detected by the system electronics (rise time ~80 nsec) in case (b) where the negative spike was due to the ionization

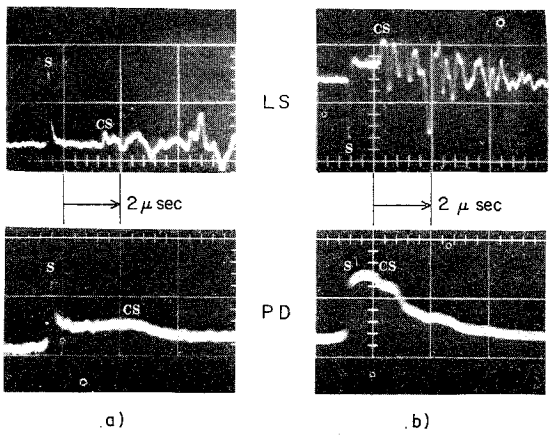

Fig. 9 Oscillogram records of signals from the laser schlieren system (LS) and the photodiode detectors (PD): a) 400 psi $2H_2+O_2$, 1 torr air, $U_s = 0.8$ cm/μsec; b) 80 g PETN, 400 psi $2H_2+O_2$, 1 torr air, $U_s = 1.34$ cm/μsec.

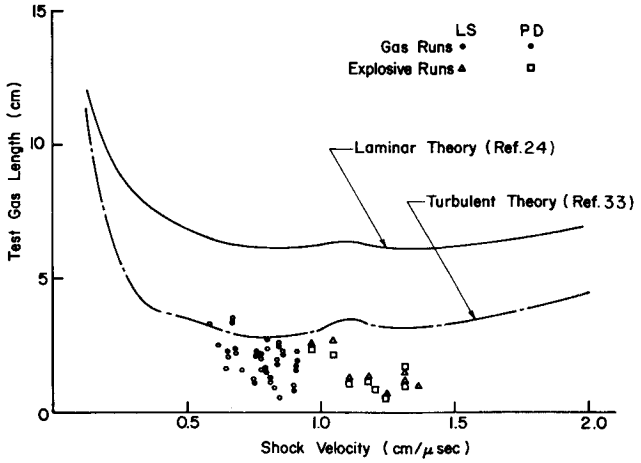

Fig. 10 Test gas lengths measured with the laser schlieren system (LS) and the photodiode detector (PD) at 3.3 m from the diaphragm, [Theories (Refs. 24, 33) give maximum expected lengths due to boundary layer losses only.]

region producing a negative refractive index gradient. (The percentages of equilibrium ionization were about 0.1 and 30 for cases (a) and (b), respectively, Ref. 32.) The photodiode detector signals also indicate a jump on the arrival of the luminous shock front. Case (a) shows a spike due to the NEQ overshoot which is absent in case (b). Radiation increases following the shock overshoot in case (a) and was shown[16] to be due to the effects of the attenuation of the shock wave on the subsequent flow properties. In case (b) radiation increases then decreases due to radiative cooling. In both cases the sudden change in slope on the radiation output profile was interpreted as the arrival of the relatively cool contact front. The test time was taken as the time between the shock S and the contact front CS in both detecting systems, which agree very well.

The test times (τ) determined from the laser-schlieren system and the photodiode detector are shown as test gas length ($l = \tau u_s$) in Fig. 10. For comparison two theoretical curves were drawn in based on Mirels' laminar[24] and turbulent[33] boundary-layer theories. The theories assume an infinitely thin contact surface. It can be seen that the test data were well below the theoretical lines showing that the actual test gas lengths were reduced by the spreading turbulent contact region[21] in addition to the boundary-layer mass-loss effects.

5. Conclusions

A theoretical and experimental study was made of the performance of a 2.54-cm-diam shock tube driven by a 20-cm-diam implosion driver with both a pure gas (stoichiometric hydrogen-oxygen $2H_2+O_2$) and this gas plus explosive PETN as drivers. A numerical analysis was carried out by solving the set of one-dimensional nonlinear partial differential equations of motion taking into account some relatively well-known losses in the tube flow such as turbulent friction and heat losses in the driver gas and boundary-layer mass loss in the driven gas. A simplified solution was developed in the form of a simple equation allowing the maximum expected shock velocity to be predicted for a given set of initial conditions. This simplified solution agreed extremely well with the exact numerical solution.

Experiments showed that the numerical analysis successfully predicted the shock wave attenuation rate. However, the magnitude of the measured shock velocities were within 12–18% below the predicted values (depending on the initial driver pressure) and within 6–8% below the corresponding predicted values for the case of an explosive driver. Average test gas lengths of about 2 cm were obtained for the gas runs at 3.3 m

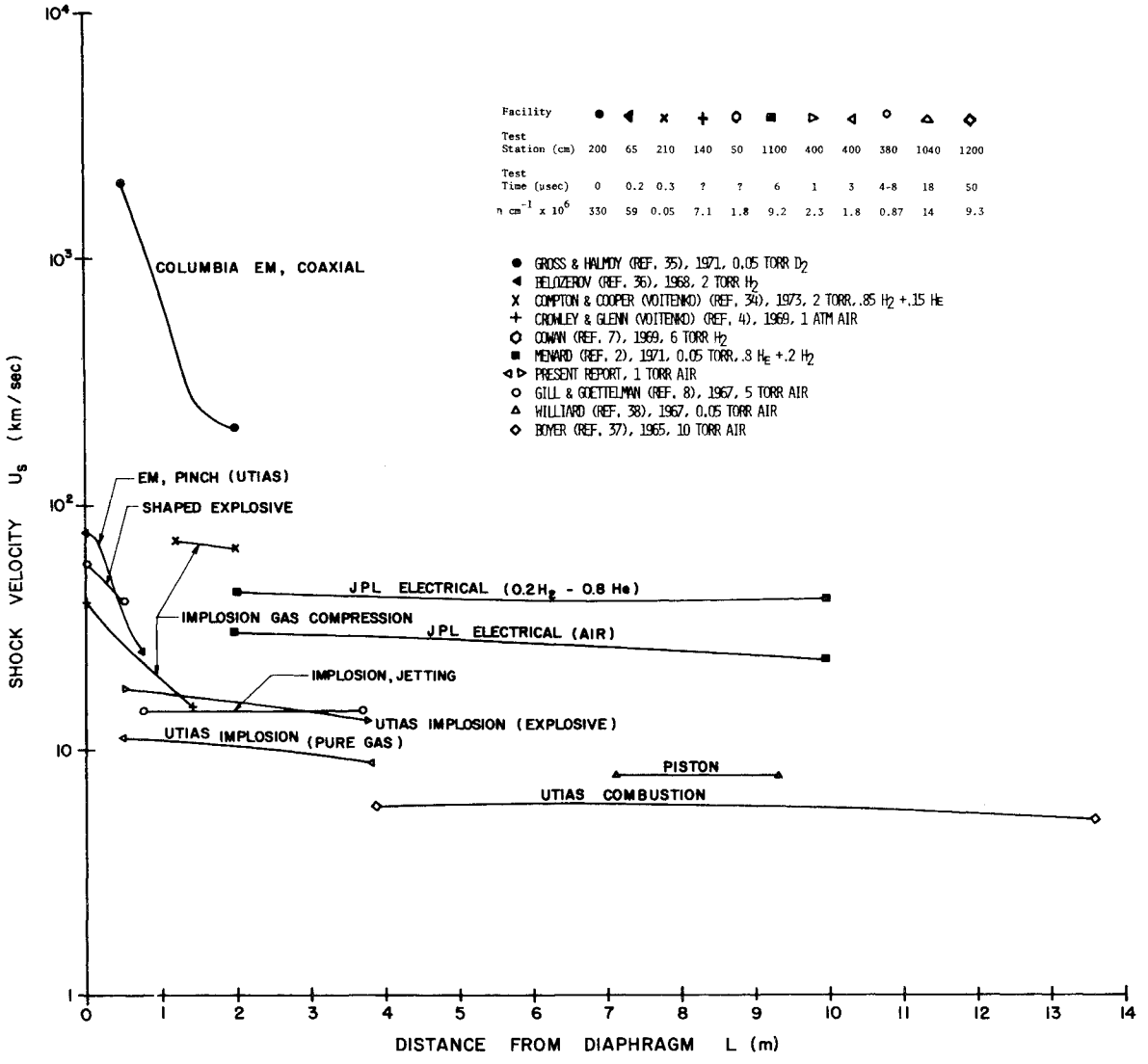

Fig. 11 Shock tube performance using a variety of driving techniques.

from the diaphragm corresponding to approximately 3-2 μsec test time for shock velocities $u_s \cong 0.6$–0.9 cm/μsec, respectively. For the explosive runs, test-gas lengths of about 1.5 cm were obtained corresponding to approximately 1 μsec test time. In general, the test gas lengths were less than the predictions from Mirels' laminar boundary-layer theory[24] by more than 50% and agreed closer with the turbulent boundary-layer theory.[33] Yet it was expected that Mirels' theory[24] might apply under the present test conditions. This shows that a better understanding of the opening flow processes and the spreading turbulent contact front are necessary to be able to predict the test times with better accuracy.

The simplified solution given here is also capable of predicting the performance of a scaled-up implosion driver. It can be shown[16] that increasing the size of the implosion driver threefold would increase the shock velocity by approximately 30% for the same tube diameter and the test time would remain approximately unchanged. The costs of scaling up the driver size to obtain this moderate gain would make it prohititive.

Finally, putting things into proper perspective, Fig. 11 compares the UTIAS implosion-driven shock-tube performance with other high-performance shock tubes. The corresponding test times obtained from each device and the energy conversion factor, η, per centimeter of test gas {the product of the channel area A_1, the initial test gas density ρ_1 (multiplying this quantity by the density ratio ρ_2/ρ_1 gives the total energy per centimeter for strong shock waves) and the square of the shock velocity U_s at the test section, divided by the total input energy} are also listed. It can be seen that the electrical and the electromagnetic drivers (solid points) generally have the highest conversion factor, that is, a higher shock velocity for a given total input energy, than the explosive drivers. This shows a better conversion efficiency from the electromagnetic type of drivers than from the explosive drivers. In view of the low conversion efficiency of the explosive drivers and the hazards of using large amounts of high explosives, it appears doubtful that explosive drivers will ever become very popular among researchers working with very high-performance shock tubes despite the fact that explosives are inexpensive compared with electrical capacitors, as noted in the Introduction. Nevertheless, the Voitenko driver has achieved the highest shock velocity with minute test times, and electrical drivers have the maximum shock velocity (with zero test time), as well as the longest test time (6 μsec) in the 50–60 km/sec range.

However, the UTIAS implosion-driven shock tube has a higher capability (10–20 km/sec) than the linear-implosion driver[8] but is well below the other types of devices such as the Voitenko compressor,[4,5,34] the shaped-explosive driver[7] and the very outstanding JPL electrical driver.[2] In addition, it should be noted that the UTIAS explosively-driven implosion driver uses only about 100 g of explosive compared with the kilograms of explosives used in other facilities. It has the advantage of being

compact, controllable and safe to operate. It is also reusable. Its potential in plasma fusion and transmutation of elemental substances, for example, graphite to diamond has still to be investigated.

References

[1] Eggers, A. J. and Cohen, N. B., "Progress and Problems in Atmosphere Entry," *Proceedings of the XVIth International Astronautical Congress,* Gauthier-Villars, Paris, 1966, pp. 339–369.

[2] Menard, W. A., "A Higher Performance Electric-Arc-Driven Shock Tube," *AIAA Journal,* Vol. 9, No. 10, Oct. 1971, pp. 2096–2098.

[3] Warren, W. R. and Harris, C. J., "A Critique of High Performance Shock Tube Driving Techniques," *Proceedings of the Seventh International Shock Tube Symposium,* edited by I. I. Glass, Univ. of Toronto Press, Toronto, Ontario, Canada, 1970, pp. 143–176.

[4] Crowley, B. K. and Glenn, H. D., "Numerical Simulation of a High Energy (Mach 120 to 40) Air-Shock Experiment," *Proceedings of the Seventh International Shock Tube Symposium,* edited by I. I. Glass, Univ. of Toronto Press, Toronto, Ontario, Canada, 1970, pp. 314–342.

[5] Voitenko, A. E., "Generation of High Speed Gas Jets," *Soviet Physics, Doklady,* Vol. 9, 1965, pp. 860–862.

[6] Titov, V. M. and Fadeenko, Yu I., "Acceleration of Solid Bodies by Cumulative Explosions," Presented at Second International Coloquium on the Gasdynamics of Explosions and Reactive Systems, Novosobirsk, U.S.S.R., 1969.

[7] Cowan, M., "Ionizing Shocks from High Explosives," Rept. SC-RR-69-320, 1969, Sandia Laboratory Research, Albuquerque, N. Mex.

[8] Gill, S. P. and Goettelman, R. C., "Implosively Accelerated Shock Tube Driver," CR-950, 1967, NASA.

[9] Savitt, J. and Stresau, R. H. F., "Velocity Attenuation of Explosive-Produced Air Shock," *Journal of Applied Physics,* Vol. 25, 1954, pp. 89–91.

[10] Schreffler, R. G. and Christian, R. H., "Boundary Disturbance in High-Explosive Shock Tubes," *Journal of Applied Physics,* Vol. 25, 1954, pp. 324–331.

[11] Glass, I. I., "Appraisal of UTIAS Implosion-Driven Hypervelocity Launchers and Shock Tubes," *Progress in Aerospace Science,* edited by D. Kuchemann, Vol. 13, Pergamon Press, New York, 1972, pp. 223–291.

[12] Glass, I. I. and Poinssot, J. C., "Implosion-Driven Shock Tube," *Proceedings of the Seventh International Shock Tube Symposium,* edited by I. I. Glass, Univ. of Toronto Press, Toronto, Ontario, Canada, 1970, pp. 343–352.

[13] Chan, S. K., Cappelli, G., and Graf, W. O., "Performance Trials of the Eight-Inch Diameter UTIAS Implosion-Driven Hypervelocity Launchers MK II and MK III," UTIAS TN 161, 1971, Univ. of Toronto, Toronto, Ontario, Canada.

[14] Czerwinski, W., "Structural Design and Development of UTIAS Implosion-Driven Launchers," UTIAS Rept. 153, 1971, Univ. of Toronto, Toronto, Ontario. Canada.

[15] Flagg, R. F., "The Application of Implosion Wave Dynamics to a Hypervelocity Launcher," UTIAS Rept. 125, 1967, Univ. of Toronto, Toronto, Ontario, Canada.

[16] Chan, S. K., "An Analytical and Experimental Study of An Implosion Driven Shock Tube," UTIAS Rept. 191, 1973, Univ. of Toronto, Toronto, Ontario, Canada.

[17] Brode, H. L., "Theoretical Description of the Performance of the UTIAS Hypervelocity Launcher," edited by A. K. Oppenheim, *Proceedings of the Second International Colloquium on Gasdynamics of Explosions and Reactive Systems, Astronautica Acta,* Vol. 15, Nos. 5 and 6, 1970, pp. 301–309.

[18] Brode, H. L., Asuno, W., Plemmons, M., Scantlin, L., and Stevenson, A., "A Program for Calculating Radiative Flow and Hydrodynamic Motion," RM-5187-PR 1967. Rand Corporation, Santa Monica, Calif.

[19] Von Neumann, J. and Richtmyer, R. D., "A Method for the Numerical Calculation of Hydrodynamic Shocks," *Journal of Applied Physics,* Vol. 21, 1950, pp. 232–237.

[20] Williams, A. C., "Propagation of the Effects of Wall Interaction in the Rarefaction Region of Shock Tube Flow," TR 6, 1955, Institute of Research, Lehigh University, Bethlehelm, Pa.

[21] Glass, I. I. and Patterson, G. N., "A Theoretical and Experimental Study of Shock Tube Flows," *Journal of the Aeronautical Sciences,* Vol. 22, 1955, pp. 73–100.

[22] Slepicka, F., "Attenuation in Shock Tubes," *Physics of Fluids,* Vol. 9, 1966, pp. 1865–1866.

[23] Emrich, R. J. and Wheeler, D. B., Jr., "Wall Effects in Shock Tube Flow," *Physics of Fluids,* Vol. 1, 1958, pp. 14–23.

[24] Mirels, H., "Test Time in Low-Pressure Shock Tubes," *Physics of Fluids,* Vol. 6, 1963, pp. 1201–1214.

[25] Mirels, H. and Mullen, J. F., "Small Perturbation Theory for Shock-Tube Attenuation and Nonuniformity," *Physics of Fluids,* Vol. 7, 1964, pp. 1208–1218.

[26] Mirels, H., "Attenuation in a Shock Tube Due to Unsteady Boundary Layer Action," Rept. 1333, 1957, NACA.

[27] Spence, D. A. and Wood, B. A., "A Review of Theoretical Treatments of Shock Tube Attenuation," *Journal of Fluid Mechanics,* Vol. 19, 1964, pp. 161–174.

[28] Mirels, H., "Correlation Formulas for Laminar Shock Tube Boundary Layer," *Physics of Fluids,* Vol. 9, 1966, pp. 1265–1272.

[29] Kemp, H. H. and Moh, T. C., "Laminar Boundary Layer Behind a Very Strong Shock Moving Into Nitrogen," *Proceedings of the Fifth International Shock Tube Symposium,* April 28–30, 1965, Naval Ordnance Lab., Silver Spring, Md.

[30] Flagg, R. F. and Mitchell, G. P., "An Optimization Study of the UTIAS Implosion-Driven Hypervelocity Launcher MK II," UTIAS 130, 1968, Univ. of Toronto, Toronto, Ontario, Canada.

[31] Roshko, A., "On Flow Duration in Low-Pressure Shock Tubes," *Physics of Fluids,* Vol. 3, 1960, pp. 835–842.

[32] Menard, W. A. and Horton, T. E., "Shock-Tube Thermochemistry Tables for High-Temperature Gases," TR 32-1408, Vol. 1, 1969, Jet Propulsion Lab., Pasadena, Calif.

[33] Mirels, H., "Shock Tube Test Time Limitation Due to Turbulent Wall Boundary Layer," *AIAA Journal,* Vol. 2, No. 1, Jan. 1964, pp. 84–93.

[34] Compton, D. L. and Cooper, D. M., "Duplication in a Shock Tube of Stagnation Region Conditions on a Jovian Atmosphere Entry Probe," Paper presented at the Ninth International Shock Tube Symposium, Stanford Univ., Stanford, Calif., July 16–19, 1973.

[35] Halmoy, E., "Production and Investigation of Very Strong Ionizing Shock Waves," Rept. 53, 1971, Columbia University Plasma Lab., New York.

[36] Belozerov, A. N., "Study of the Initial Ionization Process in a Strong Shock Tube," UTIAS Rept. 131, 1968, Univ. of Toronto, Toronto, Ontario, Canada.

[37] Boyer, A. G., "Design Instrumentation and Performance of the UTIAS 4-in. × 7-in. Hypersonic Shock Tube," UTIAS Rept. 99, 1965, Univ. of Toronto, Toronto, Ontario, Canada.

[38] Williard, J. W., "Design and Performance of the JPL Free-Piston Shock Tube," *Fifth Hypervelocity Techniques Symposium,* Univ. of Denver, Denver, Colo., March 1967.